Chinese Chemical Letters 33 (2022) 3829–3834

Contents lists available at ScienceDirect

Chinese Chemical Letters

journal homepage: www.elsevier.com/locate/cclet

Surface sulfur vacancies enhanced electron transfer over Co-ZnS quantum dots for efficient degradation of plasticizer micropollutants by peroxymonosulfate activation

Yuting Gu[a], Tingting Gao[a], Fagen Zhang[c], Chao Lu[a], Wenrui Cao[a,b], Ziwei Fu[c], Chun Hu[a], Lai Lyu[a,d,*]

[a] Key Laboratory for Water Quality and Conservation of the Pearl River Delta, Ministry of Education, Institute of Environmental Research at Greater Bay, Guangzhou University, Guangzhou 510006, China
[b] Shandong Key Laboratory of Water Pollution Control and Resource Reuse, School of Environmental Science and Engineering, Shandong University, Qingdao 266237, China
[c] School of Environmental Science and Engineering, Guangzhou University, Guangzhou 510006, China
[d] Institute of Rural Revitalization, Guangzhou University, Guangzhou 510006, China

ARTICLE INFO

Article history:
Received 22 September 2021
Revised 27 October 2021
Accepted 1 December 2021
Available online 6 December 2021

Keywords:
Peroxymonosulfate activation
Sulfur vacancy
Quantum dots
ZnS
Plasticizer

ABSTRACT

Peroxymonosulfate (PMS) activation in heterogeneous processes is a promising water treatment technology. Nevertheless, the high energy consumption and low efficiency during the reaction are ineluctable, due to electron cycling rate limitation. Herein, a new strategy is proposed based on a quantum dots (QDs)/PMS system. Co-ZnS QDs are synthesized by a water phase coprecipitation method. The inequivalent lattice-doping of Co for Zn leads to the generation of surface sulfur vacancies (SVs), which modulates the surface of the catalyst to form an electronic nonequilibrium surface. Astonishingly, the plasticizer micropollutants can be completely degraded within only tens of seconds in the Co-ZnS QDs/PMS system due to this type of surface modulation. The interfacial reaction mechanism is revealed that pollutants tend to be adsorbed on the cobalt metal sites as the electron donors, where the internal electrons of pollutants are captured by the metal species and transferred to the surface SVs. Meanwhile, PMS adsorbed on the SVs is reduced to radicals by capturing electrons, achieving effective electron recovery. Dissolved oxygen (DO) molecules are also easily attracted to catalyst defects and are reduced to $O_2^{\bullet-}$, further promoting the degradation of pollutants.

There are over 320 million tons of discarded plastics globally each year, 10% of which ultimately reach and persist in the aquatic environment [1]. Microplastics are pieces of plastic less than 5 mm in diameter [2], which may take up to several decades to decompose under natural conditions and release various harmful organic substances (such as plasticizers and antioxidants in manufacturing) during the process [3,4]. Except for the physical hazards of microplastics themselves, plasticizer bisphenol A (BPA) is an important precursor in the manufacture of plastics, which has potential environmental and human health impacts [5–8]. Peroxymonosulfate (PMS) activation, one of the most powerful advanced oxidation processes to treat organic pollutants in wastewater, generates hydroxyl radicals ($^{\bullet}OH$), sulfate radicals ($SO_4^{\bullet-}$), singlet oxygen ($^1O_2$), and other reactive oxygen species, which can effectively oxidize refractory contaminants and improve wastewater biodegradability [9–11]. Most of the current research is focused on heterogeneous catalysts such as Co_3O_4, Fe^0, and Fe_3O_4 [12–16], but an important factor limiting PMS activation is the rate-limiting step in reducing high valence metal species in the process [17]. Typically, additional PMS needs to be consumed in this step to accelerate the electron circulation in the metal species. Therefore, accelerating electron circulation is crucial in PMS activation with heterogeneous catalysts [18].

Our previous work first proposed dual reaction center (DRC) catalysts with regional differences in the electrons on the surface. In addition to H_2O_2 and persulfate, pollutants and dissolved oxygen (DO) in aquatic environments could also act as electron donors and acceptors [19–24], which suggests that the degradation capacity of pollutants by the reaction system can be enhanced by constructing the surface electron polarization of the catalyst. Recently, it has been found that the formation of surface atomic vacancies

* Corresponding author.
E-mail address: lyulai@gzhu.edu.cn (L. Lyu).

https://doi.org/10.1016/j.cclet.2021.12.004
1001-8417/

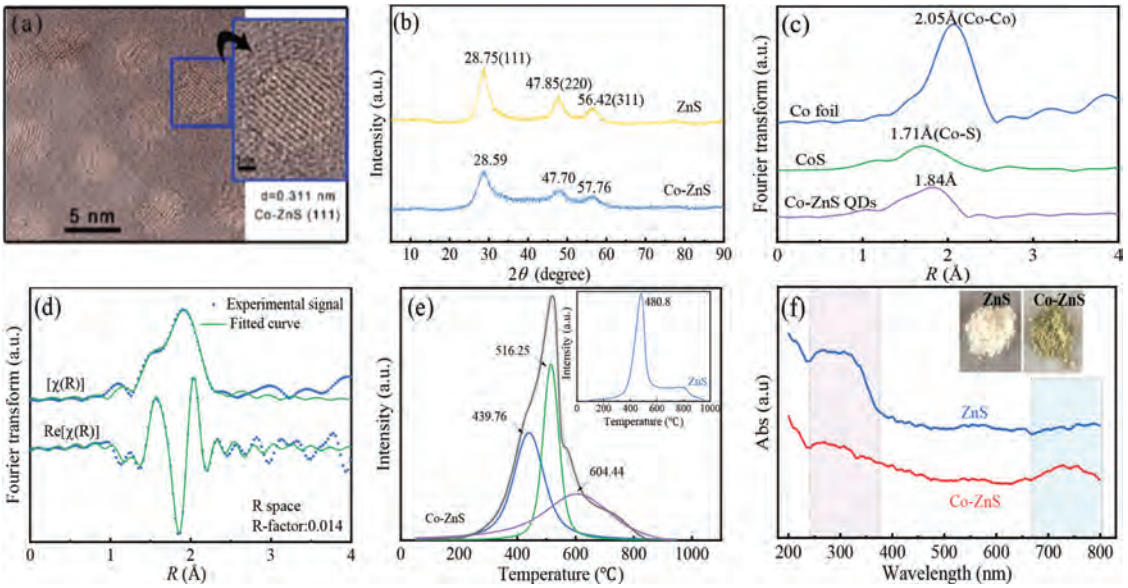

Fig. 1. (a) HRTEM images of Co-ZnS QDs. (b) The XRD pattern of Co-ZnS and ZnS. (c) Fourier transforms of k^3-weighted EXAFS oscillations obtained at the Co K-edge of Co foil, CoS and Co-ZnS QDs. (d) EXAFS curve fittings of Co-ZnS QDs on [χ(R)] and *Re*[χ(R)]. (e) H_2-temperature programmed reduction (H_2-TPR) curves of ZnS and Co-ZnS QDs. (f) UV–Vis-NIR diffuse reflection spectrum of ZnS and Co-ZnS QDs.

facilitates the construction of dual reaction centers and accelerates electron transfer [25,26]. Sulfur vacancies (SVs), similar to oxygen vacancies, are anionic defects produced on metallic sulfide surfaces by lattice sulfur detachment under specific conditions. In PMS activation, the sulfur vacancy prefers to capture an O atom in the PMS as a means of targeted electron transfer, further accelerating the conversion of the pollutant [25]. Quantum dots (QDs) receive increasing attention because of their unique characteristics and excellent photovoltaic performance, such as large specific surface area, size tunability, bound electrons and electron vacancies [27]. Due to its low toxicity, low cost and high stability, ZnS QDs are common main semiconductor material for the production of quantum dots [28].

Herein, based on the DRC theory, we first report a new strategy to generate electron-rich/poor reaction sites on the catalyst surface by constructing SVs through Co doping into the ZnS QDs lattice. It is demonstrated that in the system of cobalt-doped induced sulfur vacancies, rapid interaction between pollutants/PMS/Co-ZnS QDs can occur for electron transfer, and the pollutants are degraded by the combined action of Co^{2+} sites and free radicals, resulting in rapid oxidation of pollutants. And it is effective in the treatment of actual printing and dyeing wastewater, which provides an effective strategy with high efficiency and low energy consumption for actual wastewater treatment.

To determine the morphology and structure of the synthesized catalyst. X-ray diffraction (XRD), X-ray photoelectron spectroscopy (XPS), extended X-ray absorption fine structure (EXAFS) and other characterization methods were employed. The element maps of Co-ZnS QDs (Fig. S1 in Supporting information) confirmed the predominant existence of Zn, S, and Co elements, as well as the even dispersion of the three elements in the Co-ZnS QDs sample. The high resolution transmission electron microscopy (HRTEM) image of Co-ZnS was shown in Fig. 1a, many irregularly disconnected lattice fringes were clearly observed in the high-resolution spectrum. The lattice fringes with the same direction can be considered as a quantum dot [29], which showed that quantum dots with a diameter approximately 2.5 nm were unevenly distributed on the catalyst. In addition, it showed that the distance (0.311 nm) between adjacent lattice fringes was in good agreement with the interplanar distances of the ZnS (111) planes, which demonstrated the formation of ZnS QDs [30].

Fig. 1b showed the powder XRD pattern of the prepared catalyst. Co-ZnS QDs had three main peaks which could be attributed to the (111), (220), and (311) planes of the cubic zinc blende phase of the ZnS host material [31]. No significant changes in XRD patterns were observed when doped with Co, indicating that the catalysts retain the basic main structure after doping. Compared with the characteristic (111) reflection peak 2θ (2$\theta \approx 28.75°$) of ZnS QDs, the (111) reflection peak 2θ (2$\theta \approx 28.59°$) of Co-ZnS QDs shifted 0.16° toward the lower angle direction. Since the radius of Co^{2+} (0.058 nm) is slightly smaller than that of Zn^{2+} (0.060 nm) when Co^{2+} replaces the Zn^{2+} position in the ZnS lattice, the crystal plane spacing in the ZnS lattice decrease, and its diffraction angle shifts toward a lower angle. Co^{2+} entered the interior of the ZnS lattice in a substituted Zn^{2+} position [32]. The results of XPS in Fig. S2 (Supporting information) agreed well with previous XRD results; the doping of Co did not change the original structure of ZnS.

In Fig. 1c, the magnitude curves for the Co K-edge Fourier transformed EXAFS signals of various samples were shown. A peak at ~1.71 Å (no phase correction) was observed on the CoS sample, which was distributed to the Co−S shell. The shell (1.84 Å) of Co-ZnS QDs coincided with CoS, stating that Co(II) and the occurrence of a Co−S shell originated from the formation of Co−S bonds. In addition, to obtain finely local coordination information of the Co species in the Co-ZnS QDs, advanced fitting curves of the EXAFS signals were exhibited in Fig. 1d. In the key range of 0–2.50 Å, the fitting curves on [χ(R)] and *Re* [χ(R)] almost matched up with the experimental signals of Co-ZnS QDs, and the R-factor was ~0.014 (less than 0.020), confirming the high credibility and certainty of the fitting results. The eventually obtained fitting information was shown in Table S2 (Supporting information). There were three backscattering shells with bond distances of 2.30 Å (Co−S), 2.60 Å (Co−Zn) and 2.03 Å (Co−Co) for the Co-ZnS QDs [33]. By comparing the bond distances, it was easy to see that the Co−S shell was the first shell and the Co−Zn shell was the second shell, which indicated the formation of Co−S−Zn bonds in Co-ZnS QDs. The lattice substitution of Co easily caused the shedding of S, resulting in SVs.

Additionally, in order to detect the production of SVs on the catalyst surface, H_2-temperature programmed reduction (H_2-TPR) was further conducted to investigate the reducibility of the ZnS and Co-ZnS QDs, as shown in Fig. 1e. During the H_2-TPR process, H_2 is highly reductive, which can reduce high valent metal ions to low valent metal ions or metal atoms, and in addition, the surface oxygen and lattice oxygen ions can participate in this reduction reaction. Therefore, the results of H_2-TPR could also indicate the activity of oxygen species in catalysts [34]. For ZnS QDs, only one strong peak at 480.8 °C was due to the reduction of the high valent metal ions in ZnS QDs. With regard to the doped samples, the existence of Co improved the reduction behavior. Generally, it has been proposed that the vacancies generated in the catalyst lattice can adsorb oxygen easily. Due to the presence of defective structures, sulfur vacancies are more inclined to adsorb oxygen, resulting in the formation of active oxygen species on the catalyst surface. Therefore, many active oxygen species are formed on the catalyst surface, which can be reduced readily by H_2 at low temperature [35]. The TPR curve of Co-ZnS could be divided into three peaks. The first peak was at 439.76 °C, which was attributed to the reduction of the adsorbed oxygen species adsorbed by surface sulfur vacancies, proving the veritable existence of a large number of surface sulfur vacancies on Co-ZnS QDs with the dopant of Co species. The next two peaks at 516.25 and 604.44 °C could be assigned to the reduction of high valent metal ions Zn^{2+} and Co^{2+}, respectively [36]. The Zn^{2+} reduction temperature of Co-ZnS QDs was higher than that of ZnS QDs, so the reduction peak was shifted to high temperature with the substitution of Zn by Co, revealing that ZnS QDs less stable than Co-ZnS QDs in the reducing environment and that Co doping was critical for improving the stability of the Co-ZnS QDs structure [37].

The UV–vis-NIR diffuse reflectance spectra of the prepared sample were illustrated in Fig. 1f. The doping of Co enhanced the response of the Co-ZnS QDs in the 650–800 nm (the absorption band of Co−S at approximately 750 nm [38]) wavelength region. Starting at approximately 225 nm [39], the response of Co-ZnS QDs spectra was significantly weaker than that of the ZnS QDs. These results also demonstrated the successful doping of Co into the ZnS lattice, which weakened the response strength of ZnS.

The catalyst activity of the synthesized samples with PMS activation was evaluated by degrading BPA from an aqueous solution at natural pH. In the suspension with Co-ZnS QDs/BPA without PMS (Fig. 2a), the adsorption capacity was very inconspicuous. At the same time, BPA was barely removed in only PMS systems. Surprisingly, in the presence of PMS, the pollutant could be completely removed within tens of seconds, indicating that the Co-ZnS QDs had significant advantages over ZnS QDs (inset, Fig. 2a) in degrading BPA and activating PMS. The result confirmed that the inequivalent substitution of Co allowed the formation of an electronically nonequilibrium state on the catalyst surface, which played a crucial role in the degradation of organic pollutants by the catalyst. To further explore the influencing factors of degradation, BPA was degraded in different reaction systems. The effects of Co-ZnS QDs/PMS system about operation parameters on degradation of BPA were investigated. Fig. 2b showed the effect of different PMS dosages in BPA degradation by the suspension with Co-ZnS QDs/PMS, which showed that the activity was enhanced with increasing PMS concentration. Typically, surface hydroxyl groups readily form at the catalyst surface metal sites (Me-OH), which results in the activity of metal-containing catalysts being very susceptible to changes in pH in aqueous solution [40]. As illustrated in Fig. 2c and Fig. S4 (Supporting information), the results particularly embodied that Co-ZnS QDs successfully avoid the effects of pH and saline solutions on the degradation activity.

The catalyst stability of Co-ZnS QDs was shown in Fig. 2d. The recycling performance for the degradation of BPA in Co-ZnS QDs/PMS remained above 80% after 5 cycling runs, which showed the excellent stability of the catalyst. Furthermore, to explore the practicalities of Co-ZnS QDs, actual printing and dyeing wastewater was used to evaluate the degradation activity. Figs. 2e and f are fluorescence spectra of actual wastewater before and after (30 min) the reaction in the Co-ZnS QDs/PMS system respectively. The fluorescence intensity of the two main peaks related to the fulvic-like compounds in the suspension decreased significantly [41,42], indicating that the dissolved organic matter in the treated water was basically removed, thus significantly improving the biodegradability of the water. The results above confirmed that the Co-ZnS QDs had high efficiency, strong adaptability, and high stability.

DFT calculations were further utilized to investigate the interaction between the pollutants/PMS and the two active sites on Co-ZnS QDs. Fig. 3 presented the DFT calculations for the comparison of adsorption energy. At the electron-poor Co sites, the adsorption energy of phenol molecules ($E_{ads} = -1.09$ eV) was much lower than that of PMS, which clarified that phenol molecules could be more stably adsorbed to the Co sites. Then, we performed adsorption/reaction calculations for PMS and phenol at the sulfur vacancy. Apparently, the adsorption energy of PMS ($E_{ads} = -4.77$ eV) was the most negative at the electron-rich region SVs, indicating that PMS adsorption was most stable at the SV sites. These results theoretically suggested that pollutants tend to react in electron-poor regions at the Co site, while PMS preferred to adsorb at SVs for reaction. A stable model of the adsorption structure between them was shown in Figs. 3a and b. More DFT calculation results were shown in Figs. S5 and S6 (Supporting information). The pollutant molecule acted as an electron donor interacting directly with the electron-poor surface Co^{2+} site areas, and subsequently, electrons were transferred to the SVs. In contrary, there was a strong tendency for PMS to be adsorbed on the SV sites. When the PMS was captured by SVs, the electron-rich SVs rapidly conveyed its internal electrons to the PMS, causing a spontaneous process in which PMS decomposed into $^{\bullet}OH$ and SO_4^{2-} (or OH^- and $SO_4^{\bullet-}$). The pollutant was adsorbed on the Co^{2+} site, which was an energy-decreasing process that can proceed spontaneously, and the reaction energy barrier in the transition state was at a very low level (2.6 kcal/mol) (Fig. 3c), so the reaction could proceed quickly.

On this basis, to further explore the interfacial electron transfer process in the Co-ZnS QDs system, TEMP and BMPO capture EPR techniques were applied. As shown in Fig. 4a, in the absence of pollutants, a weak signal consisting of three characteristic peaks of TEMP-$^1O_2$ appears in the spectrum of the Co-ZnS QDs/PMS suspension, which indicated that although PMS had relatively positive adsorption energy at the Co site relative to the SVs, there was still a small part of PMS that provided electrons to the electron-poor Co^{2+} areas and is oxidized to $^1O_2$ [43,44]. After pollutants were added to the suspension, the $^1O_2$ signal almost disappeared. These results showed that the BPA molecule acted as an electron donor interacting directly with the electron-poor surface Co^{2+} site areas, attenuating the oxidation process of PMS or the addition of pollutants consuming $^1O_2$. During this process, strong BMPO-$^{\bullet}OH$ and BMPO-$SO_4^{\bullet-}$ adduct signals were also observed (Fig. 4b) [45–47], revealing that a large part of PMS was captured by the electron-rich area SVs and changed to free radicals by obtaining electrons. The intensity of the $^{\bullet}OH$ and $SO_4^{\bullet-}$ signals had no significant change after the addition of high concentrations of BPA, which demonstrated that the consumption and generation of free radicals are almost in a relatively equilibrium process. At the same time, the pollutant was also adsorbed on the cobalt metal site, providing electrons to the electron-poor area, subsequently, electrons were transferred to the SVs. The internal electrons in the SV were trapped by PMS, therefore, PMS decomposed into $^{\bullet}OH$ and $SO_4^{\bullet-}$. Consequently, on the surface of Co-ZnS QDs containing Co^{2+} sites and SVs, due to the presence of pollutants and PMS, the system

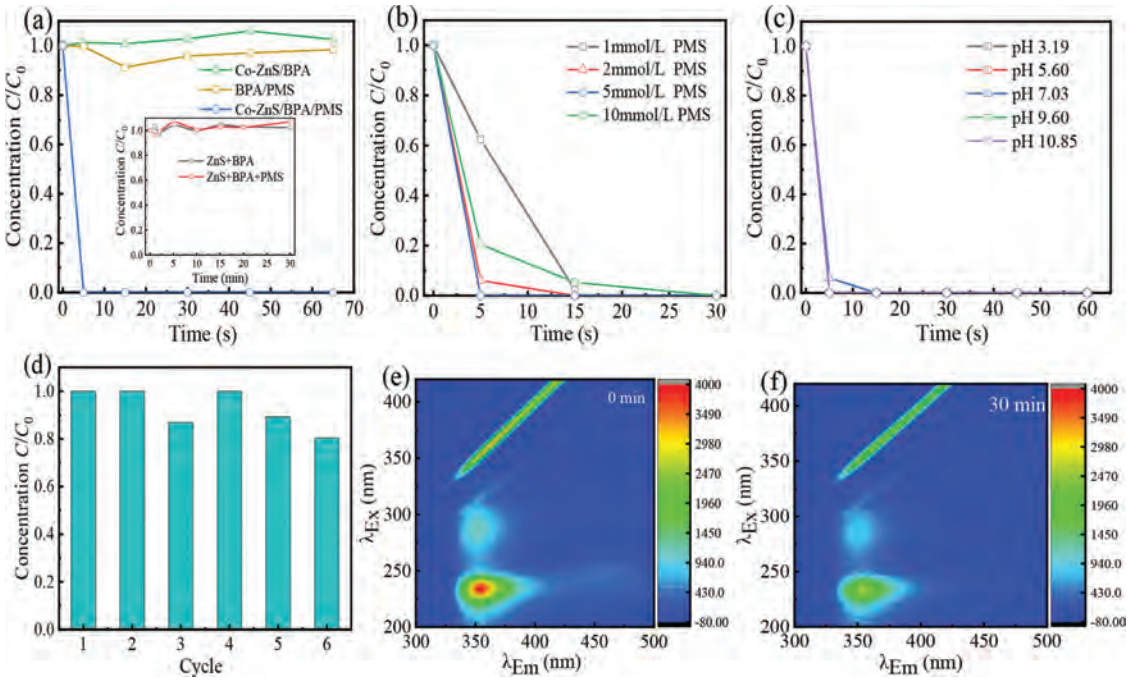

Fig. 2. (a) Degradation of BPA in ZnS QDs and Co-ZnS QDs suspensions with PMS. (b) Effect of different PMS dosages on the degradation of BPA in Co-ZnS QDs suspensions. (c) Effect of initial pH values on BPA degradation in Co-ZnS QDs/PMS. (d) The recycling performance for the degradation of BPA in Co-ZnS QDs suspensions with PMS. (e) and (f) are the 3D-EEM fluorescence spectroscopy of the actual printing and dyeing wastewater sample by the Co-ZnS QDs with PMS. Reaction conditions: [BPA] = 10 mg/L, [catalyst] = 1 g/L, [PMS] = 2 mmol/L (except b), natural pH (except c).

Adsorption types	Surface (eV)	Mol (eV)	Complex (eV)	E_{abs} (eV)
Co-PMS	-441.01	-41.83	-482.94	**-0.10**
Co-phenol	-441.01	-83.06	-525.16	**-1.09 (stable)**
SV-PMS	-441.01	-41.83	-487.61	**-4.77 (stable)**
SV-phenol	-441.01	-83.06	-525.31	-1.23

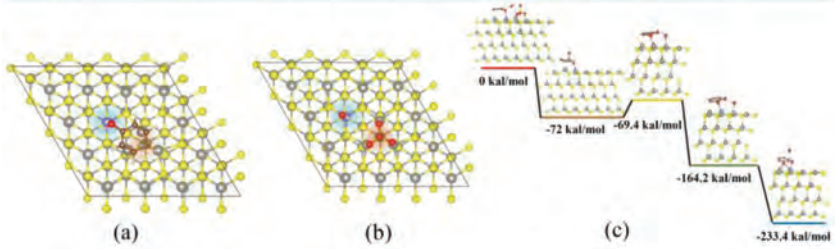

Fig. 3. (a, b) A model for stable adsorption structures of Co-Phenol and SV-PMS on Co-ZnS QDs based on DFT calculations. In addition, the results of adsorption complexation reactions of PMS and pollutants on Co^{2+} sites and SV on the surface of Co-ZnS QDs are shown (comparison of adsorption energies based on DFT calculations). Unit: eV. (c) Reaction pathways and free energies for the progressive oxidation of pollutants adsorbed on Co^{2+} sites on the Co-ZnS QDs surface based on DFT calculations.

could continuously generate free radicals and degrade pollutants. Moreover, it was generally believed that the vacancies generated in the catalyst lattice tend to adsorb oxygen. In Fig. 4c, a clear BMPO-$O_2^{\bullet-}$ signal suggested that DO molecules were also involved in the reaction [48]. DO molecules trapped electrons in the SV to form $O_2^{\bullet-}$ radicals, which also drove the pollutants to provide electrons at the Co^{2+} site, accelerating electron transfer within the system and ultimately leading to rapid degradation of the pollutants. As shown in Fig. S9 (Supporting information), it was evident that although BPA could still be completely degraded in the presence of nitrogen within 30 s, the degradation efficiency of BPA was reduced compared to degradation with oxygen, indicating that $O_2^{\bullet-}$ radicals can degrade the BPA to some extent. Fig. 4d showed the electrochemical impedance spectroscopy (EIS) results of the prepared electrodes based on the corresponding catalyst samples. The slope of EIS usually reflected the rate of electron transfer [49,50]. The EIS slops of Co-ZnS QDs /BPA and Co-ZnS QDs/BPA/PMS had almost the same slope but are significantly smaller than that of the Co-ZnS QDs, which made it clear that the addition of PMS and BPA accelerated the electron transfer rate. These results verified the experimental results that the pollutants were degraded within tens of seconds and degraded by multiple pathways.

Moreover, to demonstrate the above interface reaction mechanism, GC–MS technology was used to analyze the intermediate products in the Co-ZnS QDs/BPA/PMS system after reaction for 5 min (Fig. 4e, Fig. S7 and Table S3 in Supporting information). It was discovered that cleavage and hydroxylation products of BPA were present in the solution system after the reaction. The

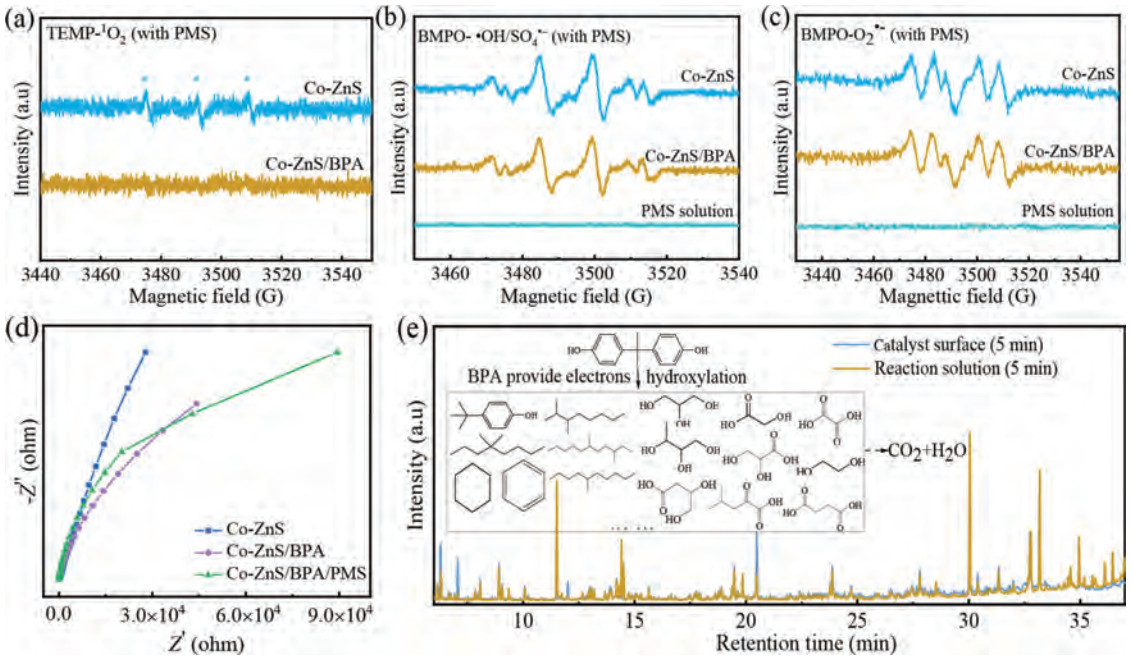

Fig. 4. TEMP spin-trapping EPR spectra for (a) $^1O_2$ in Co-ZnS QDs suspensions in the absence of PMS with/without pollutants. BMPO spin-trapping EPR spectra for (b) $^{\bullet}OH/SO_4^{\bullet-}$ and (c) $O_2^{\bullet-}$ in Co-ZnS QDs suspensions in the presence of PMS with/without pollutants. (d) Electrochemical impedance spectroscopy (EIS) of the prepared electrodes from the corresponding catalyst samples. (e) Analysis of intermediate products of BPA degradation in Co-ZnS QDs suspensions with PMS by GC–MS.

electron-donating properties of BPA allowed its direct decomposition leading to the generation of cleavage products (*e.g.*, phenol, 4–*tert*–butyl), in addition, the generation of hydroxylation products proved the further degradation of pollutants by free radicals (*e.g.*, glycerol and glycolic acid).

In summary, we first report a new strategy to generate electron-rich/poor reaction sites on the ZnS QDs surface to improve the activation efficiency of PMS. Through the lattice substitution of Co, a defective surface with electron polarization distribution is formed on the Co-ZnS QDs. The plasticizer micropollutants can be completely degraded within only tens of seconds in the surface sulfur vacancy-rich Co-ZnS QDs/PMS system. The interfacial reaction mechanism is revealed that pollutants tend to be adsorbed on the cobalt metal sites as the electron donors, where the internal electrons of pollutants are captured by the metal species and transferred to the surface SVs. Meanwhile, PMS adsorbed on the SVs is reduced to radicals by capturing electrons, achieving effective electron recovery. Dissolved oxygen (DO) molecules are also easily attracted to catalyst defects and are reduced to $O_2^{\bullet-}$, further promoting the degradation of pollutants. Thus, the Co-ZnS QDs/PMS system achieves efficient and multi-pathway degradation of pollutants. And it is effective in the treatment of actual printing and dyeing wastewater, which provides an effective strategy with high efficiency and low energy consumption for actual wastewater treatment.

Declaration of competing interest

The authors declare that they have no known competing financial interests or personal relationships that could have appeared to influence the work reported in this paper.

Acknowledgments

This work was financially supported by the National Natural Science Foundation of China (Nos. 52070046, 52122009, 51808140 and 51838005), the Introduced of Innovative R&D Team Project under the "Pearl River Talent Recruitment Program" of Guangdong Province (No. 2019ZT08L387), and the Guangdong Province Universities and Colleges Pearl River Scholar Funded Scheme (Young Scholar). The authors also appreciate the support from the BL14W1 beamline of Shanghai Synchrotron Radiation Facility (SSRF, China).

Supplementary materials

Supplementary material associated with this article can be found, in the online version, at doi:10.1016/j.cclet.2021.12.004.

References

[1] S.L. Wright, F.J. Kelly, Environ. Sci. Technol. 51 (2017) 6634–6647.
[2] W. Wei, Q.S. Huang, J. Sun, et al., Environ. Sci. Technol. 53 (2019) 2509–2517.
[3] J. Kang, L. Zhou, X. Duan, et al., Matter 1 (2019) 745–758.
[4] S. Hu, Y. Yu, Y. Guan, et al., Chin. Chem. Lett. 31 (2020) 2839–2842.
[5] J.R. Rochester, Reprod. Toxicol. 42 (2013) 132–155.
[6] L.N. Vandenberg, I. Chahoud, J.J. Heindel, et al., Environ. Health Perspect. 118 (2010) 1055–1070.
[7] B.S. Rubin, J. Steroid Biochem. Mol. Biol. 127 (2011) 27–34.
[8] Y.Q. Huang, C.K. Wong, J.S. Zheng, et al., Environ. Int. 42 (2012) 91–99.
[9] W. Tian, H. Zhang, Z. Qian, et al., Appl. Catal. B 225 (2018) 76–83.
[10] J. Yang, M. Zhu, D.D. Dionysiou, Water. Res. 189 (2021) 116627.
[11] C. Ling, S. Wu, T. Dong, et al., J. Hazard. Mater. 423 (2021) 127082.
[12] W.D. Oh, Z. Dong, T.T. Lim, Appl. Catal. B 194 (2016) 169–201.
[13] M. Zhu, L. Zhang, S. Liu, et al., Chin. Chem. Lett. 31 (2020) 1961–1965.
[14] B. Xu, W. Jiang, L. Wang, et al., Chin. Chem. Lett. 31 (2020) 2003–2006.
[15] Z. Wu, Y. Wang, Z. Xiong, et al., Appl. Catal. B 277 (2020) 119–136.
[16] S. Ullah, X. Guo, X. Luo, et al., Front. Environ. Sci. Eng. 14 (2020) 89.
[17] P. Hu, M. Long, Appl. Catal. B 181 (2016) 103–117.
[18] M. Zhang, J. He, Y. Chen, et al., Chin. Chem. Lett. 31 (2020) 2721–2724.
[19] C. Lu, K. Deng, C. Hu, L. Lyu, Front. Environ. Sci. Eng. 14 (2020) 82.
[20] L. Lyu, W. Cao, G. Yu, et al., J. Hazard. Mater. 383 (2020) 121182.
[21] L. Lyu, D. Yan, G. Yu, W. Cao, C. Hu, Environ. Sci. Technol. 52 (2018) 4294–4304.
[22] L. Lyu, L. Zhang, C. Hu, Environ. Sci. Nano 3 (2016) 1483–1492.
[23] L. Lyu, L. Zhang, Q. Wang, Y. Nie, C. Hu, Environ. Sci. Technol. 49 (2015) 8639–8647.
[24] Y. Gao, Y. Zhu, L. Lyu, et al., Environ. Sci. Technol. 52 (2018) 14371–14380.
[25] H. Zhang, C. Li, L. Lyu, C. Hu, Appl. Catal. B 270 (2020) 118874.
[26] Y. Wang, P. Zhang, T. Li, et al., J. Hazard. Mater. 408 (2021) 124818.
[27] Z. Niu, Natl. Sci. Rev. 4 (2017) 167.
[28] P. Sawetwong, S. Chairam, P. Jarujamrus, M. Amatatongchai, Talanta 225 (2021) 122077.
[29] S. Mabrouk, H. Rinnert, L. Balan, et al., J. Alloys Compd. 858 (2021) 158315.
[30] C. Song, B. Chen, Y. Chen, et al., J. Alloys Compd. 590 (2014) 546–552.

[31] V. Navakoteswara Rao, P. Ravi, M. Sathish, et al., J. Hazard. Mater. 413 (2021) 125359.
[32] S. Tomar, S. Gupta, S. Mukherjee, et al., Phys. Scripta. 96 (2021) 065802.
[33] Z. Xiong, Y. Jiang, Z. Wu, G. Yao, B. Lai, Chem. Eng. J. 421 (2021) 127863.
[34] H. Liang, Y. Hong, C. Zhu, et al., Catal. Today 201 (2013) 98–102.
[35] S. Xue, Q. Li, L. Wang, et al., Anal. Chem. 91 (2019) 2659–2666.
[36] N. Li, X. Xing, Y. Sun, et al., Front. Environ. Sci. Eng. 14 (2020) 105.
[37] S. Zhong, Y. Sun, H. Xin, et al., Chem. Eng. J. 275 (2015) 351–356.
[38] Q.Y. Tang, M.J. Yang, S.Y. Yang, Y.H. Xu, J. Hazard. Mater. 407 (2021) 124798.
[39] R. Adel, S. Ebrahim, A. Shokry, M. Soliman, M. Khalil, ACS Omega 6 (2021) 2167–2176.
[40] H. Tamura, K. Mita, A. Tanaka, M. Ito, J. Colloid Interface Sci. 243 (2001) 202–207.
[41] L. Tang, Y. Liu, J. Wang, et al., Appl. Catal. B 231 (2018) 1–10.
[42] J. Liu, Q. Yang, D. Wang, et al., Bioresour. Technol. 206 (2016) 134–140.
[43] S. Xu, H. Zhu, W. Cao, et al., Appl. Catal. B 234 (2018) 223–233.
[44] W. Cao, L. Lyu, K. Deng, et al., J. Mater. Chem. A. 8 (2020) 810–819.
[45] G.R. Buettner, Free Radicals Biol. Med. 3 (1987) 259–303.
[46] L. Lai, H. Zhou, H. Zhang, et al., Chem. Eng. J. 387 (2020) 124165.
[47] W. Li, M. Chen, Z. Zhong, M. Zhou, W. Xing, Front. Environ. Sci. Eng. 14 (2020) 102.
[48] Y. Shi, Y. Dai, Z. Liu, et al., Front. Environ. Sci. Eng. 14 (2020) 106.
[49] Y. Chen, S. Lan, M. Zhu, Chin. Chem. Lett. 32 (2021) 2052–2056.
[50] M. Li, S. Liang, Y. Wu, M. Yang, X. Huang, Front. Environ. Sci. Eng. 14 (2020) 107.